

Massively Parallel Exact Inference for Hawkes Processes

Ahmer Raza

*School of Mathematical and Statistical Sciences
Clemson University
Clemson, SC 29634, USA*

ARAZA@CLEMSON.EDU

Hudson Smith

*School of Mathematical and Statistical Sciences
Clemson University
Clemson, SC 29634, USA*

DANE2@CLEMSON.EDU

Abstract

Multivariate Hawkes processes are a widely used class of self-exciting point processes, but maximum likelihood estimation naively scales as $O(N^2)$ in the number of events. The canonical linear exponential Hawkes process admits a faster $O(N)$ recurrence, but prior work evaluates this recurrence sequentially, without exploiting parallelization on modern GPUs. We show that the Hawkes process intensity can be expressed as a product of sparse transition matrices admitting a linear-time associative multiply, enabling computation via a parallel prefix scan. This yields a simple yet massively parallelizable algorithm for maximum likelihood estimation of linear exponential Hawkes processes. Our method reduces the computational complexity to approximately $O(N/P)$ with P parallel processors, and naturally yields a batching scheme to maintain constant memory usage, avoiding GPU memory constraints. Importantly, it computes the exact likelihood without any additional assumptions or approximations, preserving the simplicity and interpretability of the model. We demonstrate orders-of-magnitude speedups on simulated and real datasets, scaling to thousands of nodes and tens of millions of events, substantially beyond scales reported in prior work. We provide an open-source PyTorch library implementing our optimizations.

Keywords: Multivariate Hawkes process, linear exponential Hawkes process, maximum likelihood estimation, parallel prefix scan, scalable inference

1 Introduction

Many natural phenomena exhibit self- and mutually-exciting behavior, whereby the occurrence of one event increases the probability of further events, either from the same source or sources that are influenced. In finance, price movements in one asset trigger further changes in the same asset and can influence movements in other assets. In seismology, a major earthquake causes aftershocks locally and can trigger earthquakes in neighboring regions. In social media, an account posting a tweet increases the account’s own likelihood of posting again and can stimulate activity in other accounts. As such, continuous time event sequences (and particularly the timing between events) encode rich information about latent influence structures.

Multivariate Hawkes processes offer a principled way to learn underlying temporal influence from continuous time event sequences. As a flexible point process family, they capture the mutual excitation of events across nodes (distinct sources of events) through the intensity function and have seen extensive success in various domains, particularly in

finance (Embrechts et al., 2011; Ait-Sahalia et al., 2015; Bacry et al., 2015; Hawkes, 2018), seismology (Ogata, 1988, 1998; Zhuang et al., 2002), epidemiology (Gerhard et al., 2017; Unwin et al., 2021; Browning et al., 2021; Chiang et al., 2022), neuroscience (Truccolo, 2016; Lambert et al., 2018), and social media activity (Zhou et al., 2013; Kobayashi and Lambiotte, 2016; Rizoiu et al., 2017b,a). The most widely used variant is the standard linear Hawkes process with a sum-of-exponentials kernel, in which past events contribute to the current intensity through linearly additive and exponentially decaying effects. Overall, a key advantage of linear Hawkes processes is that the model parameters have a direct interpretation as the influence strength of one node on another, and have also been shown to encode causal dependency between nodes (Etesami et al., 2016; Eichler et al., 2017).

Unfortunately, maximum likelihood estimation for linear Hawkes processes naively scales as $O(N^2)$ in the number of events, which severely limits their application to promising large-scale domains. The culprit is the computation of the intensity function at every event in the sequence, each of which requires summing contributions from all past events. This is a major reason for widespread adoption of the linear exponential Hawkes process, since its intensity function admits a sequential recurrence that allows for maximum likelihood inference in $O(N)$ time (Ogata, 1981). Nevertheless, scaling remains a significant issue that numerous works have sought to address, for example by exploiting sparsity in event sequences (Nickel and Le, 2021), using low-rank approximations for parameters (Zhou et al., 2013; Lemonnier et al., 2017; Bacry et al., 2020), and adopting stochastic or expectation-maximization estimation algorithms (Veen and Schoenberg, 2008; Lewis and Mohler, 2011; Kirchner, 2017). However, these approaches either rely on additional assumptions about the data or introduce simplifying approximations, and can often undermine the simplicity and interpretability of the Hawkes process. Moreover, the canonical sequential recurrence method does not enable parallelization, thus leaving the potential for efficient computation on modern Graphics Processing Units (GPUs) unexploited.

We introduce an algorithm that massively parallelizes maximum likelihood estimation for standard linear exponential Hawkes processes, which drastically alleviates its scaling issues and enables maximum likelihood inference at formerly intractable scales. Our key observation is that the sequential intensity recurrence of the linear exponential Hawkes process admits calculation using the parallel prefix scan algorithm. To our knowledge, this structure has not previously been identified or exploited for maximum likelihood inference of linear exponential Hawkes processes. Using this insight, we formulate our parallel algorithm, which uses the prefix scan to compute per-event intensities in $O(N/P + \log N)$ time, where N is the number of events and P is the number of available parallel processors (often in the hundreds or thousands for modern GPUs). Our approach naturally yields a batching scheme that keeps peak memory usage constant and allows for further parallelization across GPUs, thereby circumventing GPU memory constraints. Importantly, our method computes an exact likelihood and requires no additional assumptions or approximations to the standard linear exponential Hawkes process, thus preserving the interpretability and simplicity benefits and remaining compatible with many additional optimizations (e.g., low-rank parameterizations and consideration of event sparsity). We demonstrate our approach on simulated and real event sequences at previously infeasible scales, on the order of thousands of nodes and tens of millions of events. We observe orders of magnitude improvement in fitting time comparing against other implementations of the intensity computation. We

release an accompanying open-source PyTorch library for fitting linear exponential Hawkes processes using our approach.¹

2 Background

Consider an event sequence $\mathcal{H} = \{(t_i, m_i)\}_{i=1}^N$, where $t_i \in \mathbb{R}_{\geq 0}$ are event timestamps ordered chronologically up to time T (i.e., $0 \leq t_1 < t_2 < \dots < t_N \leq T$) and $m_i \in \{1, \dots, M\}$ is the node index for the i th event. At a particular time t , we only observe the event history up to t , denoted $\mathcal{H}_t = \{(t_i, m_i) \in \mathcal{H} : t_i < t\}$.

A temporal point process is a counting process $N(t)$ defined on $\mathbb{R}_{\geq 0}$ that counts the cumulative number of events up to time t . Temporal point processes are typically characterized by their conditional intensity function, which represents the instantaneous event rate at time t . More formally,

$$\lambda(t | \mathcal{H}_t) = \lim_{\Delta t \rightarrow 0^+} \frac{\Pr(N(t + \Delta t) - N(t) = 1 | \mathcal{H}_t)}{\Delta t}$$

For brevity, we henceforth make the conditioning on \mathcal{H}_t implicit. The intensity function for a multivariate Hawkes process is of the form $\lambda_p(t) = \mu_p + \eta_p(t)$, where $p \in \{1, \dots, M\}$ is a particular dimension, μ_p is the parameterized constant base rate, and $\eta_p(t)$ is the excitation rate. We consider the following formulation of $\lambda_p(t)$:

$$\lambda_p(t) = \mu_p + \underbrace{\sum_{j:t_j < t} \sum_{k=1}^K \alpha_{p,m_j,k} \gamma_k e^{-\gamma_k(t-t_j)}}_{\eta_p(t)} \quad (1)$$

K is the number of decay kernels that allow modeling interactions across different timescales, each with per-kernel decay rate γ_k . The parameters of interest are the per-kernel interaction matrices $\mathcal{A}_k \in \mathbb{R}_{\geq 0}^{M \times M}$, since the elements $\alpha_{p,q,k} = (\mathcal{A}_k)_{p,q}$ quantify the strength of influence of node p on node q at timescale k . This interaction structure naturally encodes causal dependencies between nodes, in the sense of directed information (Etesami et al., 2016) and Granger causality (Eichler et al., 2017). For ease of exposition, we consider a fixed base rate independent of time, although our optimizations can easily support the case of time-varying base rates $\mu_p(t)$, as our accompanying library implements.

Fitting of a Hawkes process can be done using maximum likelihood estimation, where the log-likelihood is defined as:

$$\mathcal{L}(\boldsymbol{\mu}, \mathcal{A}, \boldsymbol{\gamma}) = \sum_{i=1}^N \log \lambda_{m_i}(t_i) - \sum_{m=1}^M \int_0^T \lambda_m(t) dt \quad (2)$$

with $\boldsymbol{\mu} = (\mu_1, \dots, \mu_M)^\top$, $\mathcal{A} = \{\mathcal{A}_1, \dots, \mathcal{A}_K\}$, and $\boldsymbol{\gamma} = (\gamma_1, \dots, \gamma_K)^\top$. We impose a sparsity-inducing ℓ_1 regularization on the off-diagonal elements of each \mathcal{A}_k , since in many settings, cross-node influence is expected to be sparse while self-influence is structurally inherent (Bacry et al., 2020). The penalty is applied to elements below a certain threshold

1. Code available at <https://github.com/ahmrr/HawkesTorch>.

h , which encourages sparsity without excessively shrinking large interaction strengths. Our training objective is the per-event negative log likelihood with this penalization:

$$\text{NLL}(\boldsymbol{\mu}, \mathcal{A}) = -\frac{1}{N}\mathcal{L}(\boldsymbol{\mu}, \mathcal{A}) + \lambda_1 \mathcal{P}_{\ell_1}(\mathcal{A})$$

where $\lambda_1 \geq 0$, and:

$$\mathcal{P}_{\ell_1}(\mathcal{A}) = \sum_{k=1}^K \sum_{\substack{p,q=1 \\ p \neq q}}^M \alpha_{p,q,k} \mathbf{1}\{\alpha_{p,q,k} < h\}, \quad h > 0$$

In terms of efficiency, computation of the integral term in (2) is usually straightforward and tractable (perhaps numerically if the decay kernel or base rate parameterizations prevent analytical integration). However, computing the sequence $\{\lambda_{m_i}(t_i)\}_{i=1}^N$ for the log-sum term is time- and memory-intensive, naively scaling as $O(N^2MK)$. Therefore, our optimizations focus on scalable, parallelizable computation of the log-sum (i.e., the sequence $\{\eta_{m_i}(t_i)\}_{i=1}^N$) and its parameter gradients.

2.1 Sequential Recurrence for Intensity Computation

It is known that the Markovian nature of linear exponential Hawkes processes allows for recursively computing the likelihood (2), resulting in $O(N)$ scaling (Ogata, 1981). Due to its sequential nature, this method does not obviously allow for parallelization across the number of events N , making it difficult to exploit modern GPU hardware. However, it will be useful in developing our parallel method.

We define the quantity

$$R_p^k(t) = \sum_{j:t_j < t} \alpha_{p,m_j,k} e^{-\gamma_k(t-t_j)} \quad (3)$$

so that the excitation function (1) can be written as $\eta_p(t) = \sum_{k=1}^K \gamma_k R_p^k(t)$. We define a per-kernel state vector $\mathbf{R}_i^k = (R_1^k(t_i), \dots, R_M^k(t_i))^\top \in \mathbb{R}^M$ for $k = 1, \dots, K$ that tracks the contribution of all past events to the excitations of all M processes.

Our goal is therefore to efficiently compute the sequence $\{\mathbf{R}_i^k\}_{i=1}^N$. Let $\Delta t_i = t_i - t_{i-1}$. The above formulation naturally leads to an affine recurrence:

$$\begin{aligned} \mathbf{R}_i^k &= \sum_{j=1}^{i-1} \boldsymbol{\alpha}_{:,m_j,k} e^{-\gamma_k(t_i-t_j)} \\ &= \sum_{j=1}^{i-2} \boldsymbol{\alpha}_{:,m_j,k} e^{-\gamma_k(t_i-t_j)} + \boldsymbol{\alpha}_{:,m_{i-1},k} e^{-\gamma_k \Delta t_i} \\ &= e^{-\gamma_k \Delta t_i} \sum_{j=1}^{i-2} \boldsymbol{\alpha}_{:,m_j,k} e^{-\gamma_k(t_{i-1}-t_j)} + \boldsymbol{\alpha}_{:,m_{i-1},k} e^{-\gamma_k \Delta t_i} \\ &= e^{-\gamma_k \Delta t_i} \mathbf{R}_{i-1}^k + e^{-\gamma_k \Delta t_i} \boldsymbol{\alpha}_{:,m_{i-1},k} \end{aligned} \quad (4)$$

where the initial state is $\mathbf{R}_1^k = \mathbf{0}$, the $M \times 1$ zero column vector. This vector recurrence provides an efficient way to sequentially update the state of the intensity at each event time, and is useful for simulating Hawkes processes. Intuitively, the term $e^{-\gamma_k \Delta t_i} \mathbf{R}_{i-1}^k$ represents the exponential decay of the contributions from all events prior to t_{i-1} over the time interval Δt_i . The term $e^{-\gamma_k \Delta t_i} \boldsymbol{\alpha}_{:,m_{i-1},k}$ represents the influence of the event at t_{i-1} (which was of type m_{i-1}), since the jump vector $\boldsymbol{\alpha}_{:,m_{i-1},k}$ gives the immediate impact on all process intensities at t_{i-1} , and this impact then decays exponentially until just before t_i .

2.2 Parallel Prefix Scan

This section provides a brief introduction to the parallel prefix scan algorithm (henceforth simply prefix scan) that we use in our approach. Given a sequence $\{a_1, a_2, \dots, a_n\}$, the prefix scan allows computing the sequence of cumulative aggregates $\{p_i\}_{i=1}^n$, each defined as:

$$p_i = \bigodot_{j=1}^i a_j$$

where \odot is an arbitrary associative operator (e.g., matrix multiplication) that is not necessarily commutative. Prefix scans can be used to calculate recurrences of the form $p_i = p_{i-1} \odot a_i$ that can be done sequentially in $O(n)$ time, except that a prefix scan admits significant parallelization.

Two canonical prefix scan algorithms are the Hillis-Steele scan (Hillis and Steele, 1986) and the Blelloch scan (Blelloch, 1990). The Hillis-Steele scan has $O(n/P \cdot \log n + \log n)$ time complexity, offering high parallelism and best performance when $n \leq P$, where P is the number of available parallel processors. Conversely, the Blelloch scan has $O(n/P + \log n)$ time complexity, asymptotically performing no more operations than the sequential implementation albeit with less parallelism. This makes it preferable when $n \gg P$, as in our setting where the number of events can reach millions, while GPUs provide only thousands of cores. Therefore, we adopt the Blelloch implementation of the prefix scan.

Figure 1 presents an illustration of the Blelloch scan, which consists of two stages. In the upsweep stage, the algorithm starts at the leaves of a binary tree and computes pairwise combinations of these elements in parallel. These intermediate results are then combined pairwise at the next level of the tree, and so on, until the root node is reached, storing the cumulative value $p_n = \bigodot_{j=1}^n a_j$. In the downsweep stage, the algorithm reverses this process. The root node is initialized to the identity element of \odot , and at each node, the current prefix value is propagated down to reconstruct the prefix scans for its children. Because of this binary tree-like structure, the algorithm can only operate on sequences whose length is a power of two, so input sequences must be padded with the appropriate identity element. When parallelized across P concurrent processors, the time complexity of this algorithm is $O(n/P + \log n)$, and when $n/P \geq \log P$ the complexity reduces to $O(n/P)$, which is the optimal speedup over the sequential implementation (Blelloch, 1990).

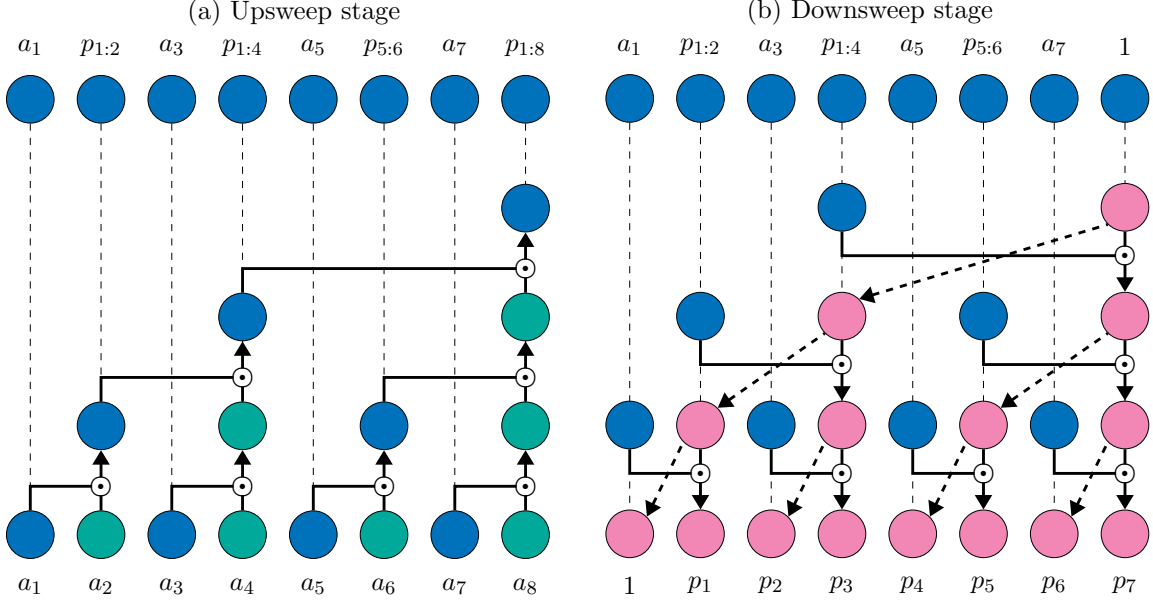


Figure 1: A visualization of the Blelloch scan upsweep and downsweep stages performed on an example input sequence $\{a_i\}_{i=1}^8$. Here, $p_{i:j} = \bigodot_{k=i}^j a_k$ denotes a partial aggregate.

3 Methods

The crux of our approach is reformulating the affine recurrence (4) to an equivalent matrix product form using state augmentation. This transforms the affine recurrence into a linear one in a higher dimension, which will admit application of the prefix scan algorithm. Define the augmented state vector $\tilde{\mathbf{R}}_i^k \in \mathbb{R}^{M+1}$ as:

$$\tilde{\mathbf{R}}_i^k = \begin{pmatrix} \mathbf{R}_i^k \\ 1 \end{pmatrix} \quad (5)$$

Let I_M be the $M \times M$ identity matrix and $\mathbf{0}^\top$ be the $1 \times M$ zero row vector. We define the block transition matrices $\mathbf{M}_i^k \in \mathbb{R}^{(M+1) \times (M+1)}$ as:

$$\mathbf{M}_i^k = \begin{pmatrix} e^{-\gamma_k \Delta t_i} I_M & e^{-\gamma_k \Delta t_i} \boldsymbol{\alpha}_{:,m_{i-1},k} \\ \mathbf{0}^\top & 1 \end{pmatrix} \quad (6)$$

where $\mathbf{M}_1^k = I_{M+1}$. The recurrence for the augmented state vector is linear:

$$\tilde{\mathbf{R}}_i^k = \mathbf{M}_i^k \tilde{\mathbf{R}}_{i-1}^k \quad (7)$$

Unrolling this recurrence gives the matrix product form $\tilde{\mathbf{R}}_i^k = \mathbf{P}_i^k \tilde{\mathbf{R}}_0^k$, where $\mathbf{P}_i^k = \mathbf{M}_i^k \mathbf{M}_{i-1}^k \dots \mathbf{M}_1^k$, so computing $\{\tilde{\mathbf{R}}_i^k\}_{i=1}^N$ amounts to computing the products $\{\mathbf{P}_i^k\}_{i=1}^N$.

A key feature of this formulation is that each product of $(M+1) \times (M+1)$ transition matrices is done in $O(M)$ operations rather than the usual $O(M^3)$. To see this, consider the product of two matrices in the same format as \mathbf{M}_i^k , each defined by scalars s_A , s_B and

vectors $\mathbf{v}_A, \mathbf{v}_B$:

$$\begin{pmatrix} s_A I_M & \mathbf{v}_A \\ \mathbf{0}^\top & 1 \end{pmatrix} \begin{pmatrix} s_B I_M & \mathbf{v}_B \\ \mathbf{0}^\top & 1 \end{pmatrix} = \begin{pmatrix} s_A s_B I_M & s_A \mathbf{v}_B + \mathbf{v}_A \\ \mathbf{0}^\top & 1 \end{pmatrix}$$

The resulting matrix retains the same structure, defined by a new scalar $s_{AB} = s_A s_B$ and a new vector $\mathbf{v}_{AB} = s_A \mathbf{v}_B + \mathbf{v}_A$. This special sparsity structure also means that each matrix can be stored using $O(M)$ memory instead of $O(M^2)$ for a dense matrix, storing only the pair $\tilde{\mathbf{M}}_i^k = (e^{-\gamma_k \Delta t_i}, e^{-\gamma_k \Delta t_i} \boldsymbol{\alpha}_{:,m_{i-1},k})$. This formulation lends itself to the prefix scan algorithm, where the input is the sequence of sparse transition matrices $\{\tilde{\mathbf{M}}_i^k\}_{i=1}^N$, and the associative operation between two sparse matrices is precisely the $O(M)$ matrix multiplication described above:

$$(s_A, \mathbf{v}_A) \odot (s_B, \mathbf{v}_B) = (s_A s_B, s_A \mathbf{v}_B + \mathbf{v}_A)$$

Using the intensity states (3), the intensity at a time in between events $t \in [t_i, t_{i+1})$ can also be computed, which is useful for visualization, diagnostics, and simulation. The intensity function can be decomposed as:

$$\lambda_p(t) = \mu_p + \sum_{k=1}^K \gamma_k e^{-\gamma_k(t-t_i)} R_p^k(t_i^-) + \sum_{k=1}^K \alpha_{p,m_i,k} \gamma_k e^{-\gamma_k(t-t_i)}$$

That is, $\lambda_p(t)$ can be calculated using the precomputed state vector \mathbf{R}_i for the event that happens right before time t .

The reader may recognize that a prefix scan can simply be applied to the intensity formula (1), which becomes apparent by rewriting the excitation at each event time as:

$$\eta_p(t_i) = e^{-\gamma_k t_i} \sum_{j=1}^{i-1} \sum_{k=1}^K \alpha_{p,m_j,k} \gamma_k e^{\gamma_k t_j}$$

In practice, this is numerically unstable for large event sequences due to the summation of exponentials, which blows up and quickly becomes floating-point infinity, since the $e^{-\gamma_k t_i}$ is multiplied afterwards. Rescaling by a large number (e.g., T) does not solve the issue either, as the summation underflows to zero. Using the recurrence formulation avoids this issue entirely by using the inter-event times Δt_i , keeping exponents small.

3.1 Efficient Parameter Gradients

While the PyTorch automatic differentiation engine (autograd) can automatically compute the gradients of the log-likelihood, the Blelloch scan implementation leads to a complex compute graph that autograd traverses inefficiently. The upsweep and downsweep each contain $O(N)$ nodes across their $\lceil \log_2 N \rceil$ tree levels, and autograd incurs per-node interpreter overhead by visiting each node sequentially, without exploiting the within-level parallelism available at each level.

To avoid this inefficiency, we derive the parameter gradients manually, and compute them using prefix scans on state vectors analogous to the intensity computation. From

the log-likelihood definition (2), we can write its derivatives with respect to the relevant parameters as:

$$\frac{\partial \mathcal{L}}{\partial \mu_p} = \sum_{i:m_i=p} \frac{1}{\lambda_{m_i}(t_i)} - T \quad (8)$$

$$\frac{\partial \mathcal{L}}{\partial \alpha_{p,q,k}} = \sum_{i:m_i=p} \frac{\gamma_k K_q^k(t_i)}{\lambda_{m_i}(t_i)} - \sum_{i:m_i=q} \left(1 - e^{-\gamma_k(T-t_i)}\right) \quad (9)$$

$$\frac{\partial \mathcal{L}}{\partial \gamma_k} = \sum_{i=1}^N \left[\frac{(1 - \gamma_k t_i) R_{m_i}^k(t_i) + \gamma_k L_{m_i}^k(t_i)}{\lambda_{m_i}(t_i)} \right] - \sum_{m=1}^M \sum_{i=1}^N \alpha_{m,m_i,k} (T - t_i) e^{-\gamma_k(T-t_i)} \quad (10)$$

where each component of the per-kernel gradient state vectors $\mathbf{K}_i^k = (K_1^k(t_i), \dots, K_M^k(t_i))^\top \in \mathbb{R}^M$ and $\mathbf{L}_i^k = (L_1^k(t_i), \dots, L_M^k(t_i))^\top \in \mathbb{R}^M$ are:

$$K_q^k(t) = \sum_{j:t_j < t} \delta_{m_j,q} e^{-\gamma_k(t-t_j)}$$

$$L_p^k(t) = \sum_{j:t_j < t} \alpha_{p,m_j,k} t_j e^{-\gamma_k(t-t_j)}$$

This formulation similarly yields affine recurrences for the state vectors:

$$\mathbf{K}_i^k = e^{-\gamma_k \Delta t_i} \mathbf{K}_{i-1}^k + e^{-\gamma_k \Delta t_i} \mathbf{e}_{m_{i-1}} \quad (11)$$

$$\mathbf{L}_i^k = e^{-\gamma_k \Delta t_i} \mathbf{L}_{i-1}^k + t_{i-1} e^{-\gamma_k \Delta t_i} \boldsymbol{\alpha}_{:,m_{i-1},k} \quad (12)$$

Or, equivalently, in linear matrix product form using state augmentation:

$$\begin{aligned} \tilde{\mathbf{K}}_i^k &= \begin{pmatrix} \mathbf{K}_i^k \\ 1 \end{pmatrix} = \begin{pmatrix} e^{-\gamma_k \Delta t_i} I_M & e^{-\gamma_k \Delta t_i} \mathbf{e}_{m_{i-1}} \\ \mathbf{0}^\top & 1 \end{pmatrix} \begin{pmatrix} \mathbf{K}_{i-1}^k \\ 1 \end{pmatrix} \\ \tilde{\mathbf{L}}_i^k &= \begin{pmatrix} \mathbf{L}_i^k \\ 1 \end{pmatrix} = \begin{pmatrix} e^{-\gamma_k \Delta t_i} I_M & e^{-\gamma_k \Delta t_i} t_{i-1} \boldsymbol{\alpha}_{:,m_{i-1},k} \\ \mathbf{0}^\top & 1 \end{pmatrix} \begin{pmatrix} \mathbf{L}_{i-1}^k \\ 1 \end{pmatrix} \end{aligned}$$

where $\mathbf{e}_i \in \{0, 1\}^M$ denotes the vector of 0's with a single 1 at the i th position. Note that the derivative with respect to $\alpha_{p,q,k}$ depends only on q and k , so the given sequence can be computed to obtain a vector of derivatives with respect to a particular q component, reused across all p .

3.2 Time Complexity Analysis and Batching

We discuss the general time complexity of our method, both in terms of memory and compute; specifically, we examine the complexity of the one prefix scan required in the forward pass and the two in the backward pass. Across the kernel dimension K , the cost of each associative matrix multiplication is $O(KM)$, meaning that the prefix scan operates in time $O(KMN/P)$ for P parallel processors. For each prefix scan, the peak memory required for storing the compressed prefix matrices is $O(KMN)$. This may be prohibitive when fitting very large event sequences, e.g. $M \gtrsim 10^3$ and $N \gtrsim 10^6$. We thus outline a

method for calculating gradients in a batched manner, so as to guarantee constant peak memory usage.

Consider partitioning the sequence \mathcal{H} into B batches. Let $\mathcal{I} = \{1, \dots, N\}$ denote the index set for all events, and let

$$\mathcal{I}_b = \{(b-1)N_b + 1, (b-1)N_b + 2, \dots, bN_b\}$$

denote the index set for a particular batch $b = 1, \dots, B$, where N_b is the size of batch b . Since we are interested in bounding the peak memory usage, all batch sizes will be the same and will be collectively referred to as N_b without substituting a value for b .

In the forward pass, for each batch b , we can independently compute the per-batch states $\{\mathbf{R}_i^k\}_{i \in \mathcal{I}_b}$ using the final state of the previous batch $\mathbf{R}_{(b-1)N_b}^k$, since for any index $l < i$:

$$\tilde{\mathbf{R}}_i^k = \mathbf{P}_i^k \tilde{\mathbf{R}}_0^k = \left[\prod_{j=l+1}^i \mathbf{M}_j^k \right] \tilde{\mathbf{R}}_l^k$$

Similarly, for each batch b in the backward pass, we can compute $\{\mathbf{K}_i^k\}_{i \in \mathcal{I}_b}$ and $\{\mathbf{L}_i^k\}_{i \in \mathcal{I}_b}$ using the previous batch states $\mathbf{K}_{(b-1)N_b}^k$ and $\mathbf{L}_{(b-1)N_b}^k$, respectively. A key benefit of this batching approach is that each batch depends on the previous only through a single state. Therefore, the products for each batch can be computed independently, perhaps parallelized across different GPUs.

Importantly, this batching scheme does not approximate gradients: they are computed exactly over the entire sequence, and batching is used purely to control memory consumption. To illustrate the approach, Algorithm 1 presents the full training procedure for the unbatched case. For clarity, we treat the kernel dimension k as independent and vectorized, so no explicit loop over k is included. The batched version of the procedure is a straightforward extension, and is given in Appendix A.

3.3 Advantages and Limitations

A key advantage of our approach is that it does not make any simplifying assumptions or approximations, and computes exact likelihood and gradients. It is therefore easily compatible with many existing optimizations, such as optimizations for sparse event sequences (Nickel and Le, 2021) and low-rank parameterizations (Bacry et al., 2020). However, our method relies on parallelism, so if a highly parallel device (i.e., GPU or many CPU cores) is not available, it is unlikely to provide significant speedup. Moreover, prefix scans are most efficient at large scales, so our approach offers little benefit for small event sequences. In the following section, we evaluate the scaling of our approach on synthetic data, and comparison studies demonstrating the typical conditions under which our method outperforms other implementations.

4 Results

We evaluate our method on both simulated and real-world datasets to assess its performance, scalability, and practical utility. Because our algorithm does not alter the likelihood or

Algorithm 1: Massively parallelizable training of multivariate Hawkes processes

define PrefixScan $_{\odot}(\cdot)$ **from** Section 2.2
for each epoch ℓ **do**
 FORWARD PASS
 $\{(\mathbf{R}_i^k, *)\}_{i \in \mathcal{I}} \leftarrow \text{PrefixScan}_{\odot} \left(\{(e^{-\gamma_k \Delta t_i}, e^{-\gamma_k \Delta t_i} \boldsymbol{\alpha}_{:, m_{i-1}})\}_{i \in \mathcal{I}} \right)$
 $\boldsymbol{\lambda}(t_i) \leftarrow \boldsymbol{\mu} + \sum_{k=1}^K \gamma_k \mathbf{R}_i^k, \forall i \in \mathcal{I}$
 $\mathcal{L} \leftarrow \sum_{i \in \mathcal{I}} \log \lambda_{m_i}(t_i)$
 store $\{\lambda_{m_i}(t_i)\}_{i \in \mathcal{I}}, \{R_{m_i}(t_i)\}_{i \in \mathcal{I}}$ for backward pass
 BACKWARD PASS
 $\{(\mathbf{K}_i^k, *)\}_{i \in \mathcal{I}} \leftarrow \text{PrefixScan}_{\odot} \left(\{(e^{-\gamma_k \Delta t_i}, e^{-\gamma_k \Delta t_i} \mathbf{e}_{m_{i-1}})\}_{i \in \mathcal{I}} \right)$
 $\{(\mathbf{L}_i^k, *)\}_{i \in \mathcal{I}} \leftarrow \text{PrefixScan}_{\odot} \left(\{(e^{-\gamma_k \Delta t_i}, e^{-\gamma_k \Delta t_i} t_{i-1} \boldsymbol{\alpha}_{:, m_{i-1}})\}_{i \in \mathcal{I}} \right)$
 $\nabla \alpha_{p,q,k} \leftarrow$ using Equation (9) and $\{\mathbf{K}_i^k\}_{i \in \mathcal{I}}$
 $\nabla \gamma_k \leftarrow$ using Equation (10) and $\{\mathbf{L}_i^k\}_{i \in \mathcal{I}}, \{R_{m_i}(t_i)\}_{i \in \mathcal{I}}$
 $\nabla \mu_p \leftarrow$ using Equation (8) and $\{\lambda_{m_i}(t_i)\}_{i \in \mathcal{I}}$
 $\mu_p, \alpha_{p,q,k}, \gamma_k \leftarrow \text{OptimizerStep}(\mu_p, \alpha_{p,q,k}, \gamma_k, \nabla \mu_p, \nabla \alpha_{p,q,k}, \nabla \gamma_k, \text{lr})$

gradients, we focus our empirical evaluation on computational efficiency, and include a single numerical example confirming the equivalence. Using synthetic data, we study scaling behavior and conduct an ablation study, comparing against different implementations of the intensity. We then demonstrate performance on real datasets that were formerly intractable with standard approaches, namely MemeTracker and Chicago crime data, to show both the scalability and interpretability of our approach. All experiments were run primarily on an Nvidia A100 80GB GPU. When comparing against CPU implementations, we used 64 cores of the fastest available CPU on our cluster, the Intel Xeon Platinum 8580.

4.1 Scaling on Synthetic Data

We now study the scaling of our algorithm on massive simulated event sequences. Here, we use $\gamma = 1.5$ and simulate from a hub-and-spoke influence network, where a single row of the interaction matrix \mathcal{A} is set to 0.1, and the base rate μ_p of the single hub node is 0.1. We consider event sequences of length equal to powers of two, since the prefix scan internally pads shorter sequences to the next power of two. The sequence lengths range from $N = 2^{10}$ to $N = 2^{26}$ (i.e., $N \sim 10^3$ to $N \sim 6.7 \times 10^7$), and the number of nodes ranges from $M = 125$ to 2000, doubling at each step. We use $K = 3$ exponential decay kernels with parameterized decay rates. All runs are performed on the GPU, and each sequence was fitted for 1000 epochs, with a maximum allowed wall time of 72 hours.

Figure 2 shows time and memory scaling across the simulated sequences. As expected from theoretical scaling, the epoch time and memory grow linearly with the number of events (and the number of nodes) for larger event sequences. In the small N regime, scaling is sublinear due to vacant parallel cores on the GPU, and then transitions to linear once all the cores saturate. Once batching begins, the memory usage peaks at 47.31 GiB, which can be adjusted via the batch size to match the target hardware. The performance curves are

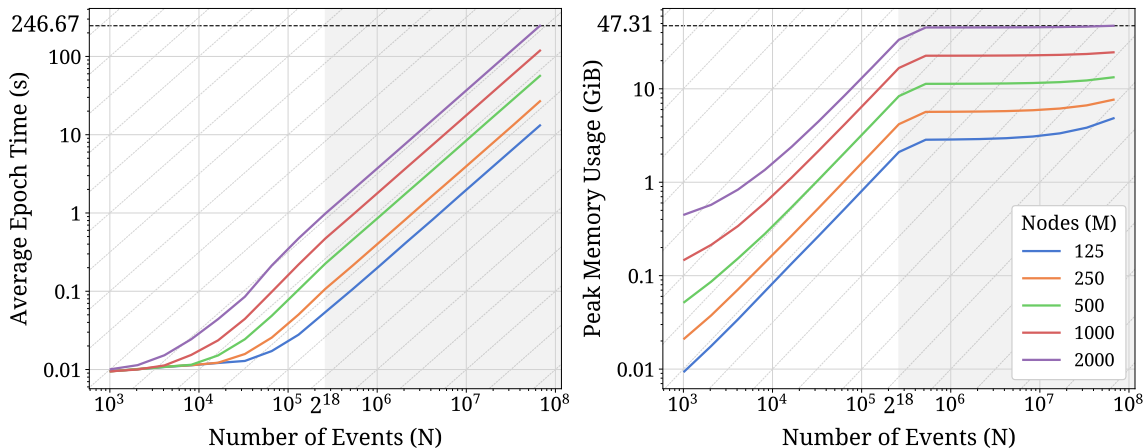


Figure 2: Scaling of our method across various sequence lengths, showing average epoch time (left) and peak memory usage (right). The gray region indicates where batching is enabled to maintain constant memory (with batch size $2^{19} = 524,288$). Dashed black lines indicate the maximum epoch time and memory usage across all runs, respectively. Diagonal gridlines with unit power (slope 1 on log-log plot) are shown for reference.

remarkably stable due to the prefix scan: each doubling of N causes a consistent doubling in the average epoch time, which peaks at 246.67 seconds.

4.2 Comparison to Other Likelihood Computation Methods

On the same synthetic data, we conduct an ablation study comparing different implementations of the likelihood computation. The naive baseline implementation, which scales quadratically in the number of events, involves directly computing the sum over previous events for each intensity $\lambda_{m_i}(t_i)$. The sequential implementation uses the recurrence formulas (4), (11), and (12), and is tested on both the GPU and CPU. The CPU version is given 64 CPU cores, although there is no parallelization and thus negligible benefit from providing more cores. Finally, we test our prefix scan-based algorithm both using PyTorch’s default autograd gradients and our manual gradient computation. All runs are fitted for 1000 epochs and limited to 24 hours.

Figure 3 presents the per-epoch time and peak memory usage of each ablation configuration. The naive method runs in quadratic time and is heavily memory-bound, terminating within 10^5 events. The sequential methods (both on the GPU and CPU) have the expected linear runtime and constant peak memory usage, but the constant factor is very large and, thus, the sequential implementations terminate early. The single-core CPU implementation outperforms the equivalent GPU version because the sequential intensity computation is not parallelizable, so running on the GPU incurs significant overhead and suffers from weak single-core performance. The prefix scan implementation with PyTorch autograd gradients scales significantly better than the other methods, but does not provide an easy way to do batching and, therefore, is memory-limited. Moreover, storing and traversing the complicated compute graph results in slowdown, with the empirical scaling also being superlinear.

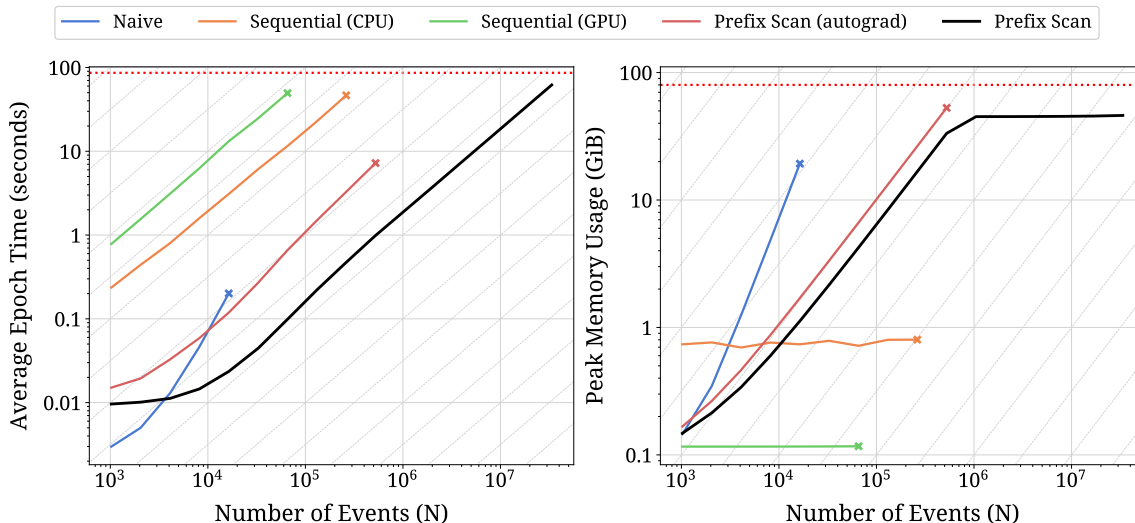


Figure 3: Comparison between our method (black) and other implementations of the intensity computation. The red dotted lines indicate the 24-hour walltime limit (86.4 seconds per epoch for 1000 epochs) and the maximum available memory (80 GiB), respectively. Crosses indicate that the next run either ran out of memory or exceeded 24 hours.

Finally, the full implementation using the prefix scan is, by far, the most performance efficient, being orders of magnitude faster than the alternative implementations and scalable to arbitrary N due to the constant memory usage.

4.3 Parameter Recovery Study

While estimation accuracy is not the primary focus of this work, we include a small synthetic experiment to verify that our proposed algorithm preserves standard Hawkes parameter recovery behavior. We simulate event sequences from a single-kernel multivariate Hawkes process using Ogata’s thinning algorithm (Ogata, 1981). For all dimensions p , the base rate is fixed to $\mu_p = 0.001$, and a single exponential decay kernel with rate $\gamma = 1.0$ is used. We vary the number of dimensions $M \in \{10, 50, 100, 250, 500, 1000\}$ while fixing the total number of events to $N = 1,000,000$. The interaction matrix \mathcal{A} is generated from a sparse directed scale-free graph (Bollobás et al., 2003; Barabási, 2009). The penalty weight and hinge point are set to $\lambda_1 = 0.1$ and $h = 0.05$, respectively. The synthetic event sequences are then fitted using a single-kernel Hawkes model with the Adam optimizer, with 1000 epochs and a learning rate of 0.05.

Table 1 reports the per-event log-likelihood and relative root mean squared error (RRMSE) of the estimated parameters with respect to their true values. For a parameter vector θ and estimate $\hat{\theta}$, the RRMSE is defined as

$$\text{RRMSE}(\theta, \hat{\theta}) = \sqrt{\frac{\sum_i (\theta_i - \hat{\theta}_i)^2}{\sum_i \theta_i^2}}$$

where the sum is taken over all entries of the corresponding parameter.

Nodes	N/M^2	Log-Lik.	RRMSE		
			μ	\mathcal{A}	γ
10	100000	-2.017	1.71×10^{-3}	1.80×10^{-2}	1.17×10^{-1}
50	400	-2.828	7.18×10^{-3}	1.64×10^{-2}	8.36×10^{-3}
100	100	-3.120	1.96×10^{-2}	2.76×10^{-2}	1.09×10^{-2}
250	16	-4.536	4.72×10^{-2}	3.89×10^{-2}	9.36×10^{-3}
500	4	-4.712	1.34×10^{-1}	1.20×10^{-1}	1.51×10^{-2}
1000	1	-5.805	4.01×10^{-1}	6.22×10^{-1}	7.30×10^{-3}

Table 1: Synthetic parameter recovery results. Per-event log-likelihood is reported, and N/M^2 is the number of events per interaction parameter.

Across all settings, the decay rate γ is consistently estimated with less than 2% relative error. When the number of events per interaction parameter is moderate ($N/M^2 \geq 16$), both the base rate μ and interaction matrix \mathcal{A} are recovered with RRMSE below 5%. However, highly underdetermined settings ($N/M^2 = 1$ and 4) exhibit much higher relative errors; for example, the RRMSE reaches 62.2% when $M = 1000$. In these cases, most interactions are weakly informed by the data, and the ℓ_1 penalty further shrinks weakly supported elements of \mathcal{A} toward zero. Nonetheless, the parameters remain well-recovered in most scenarios, and the model still captures the global dynamics of the process.

4.4 MemeTracker Data

To examine the runtime performance of our approach on real information cascades, we use various subsets of the MemeTracker dataset Leskovec et al. (2009) as curated by Gomez Rodriguez et al. (2013). The full dataset consists of 34,547,727 unique memes posted on 5000 of the most active websites between March 2011 and February 2012. Memes are grouped into 178 cascades based on shared keywords in their text content, where each event in the cascade corresponds to a meme being posted on a specific website at a particular time. We apply our method to ten representative subsets spanning approximately 6.4×10^4 to 3.2×10^7 events, each using $K = 3$ decay kernels and trained for 1000 epochs.

Results for all subsets are reported in Table 2. For comparison, we also include average per-epoch runtimes on four MemeTracker subsets reported by Nickel and Le (2021), who demonstrate speedup by using a low-rank parameterization and exploiting sparsity in event sequences. As emphasized earlier, our approach exclusively targets efficient likelihood computation, and is therefore complementary in nature to many existing optimizations. Hence, this comparison is intended to highlight the potential gains from likelihood speedups alone, without supplementary optimizations.

Across the four subsets considered by Nickel and Le (2021), we observe approximately an order-of-magnitude reduction in runtime per epoch, with smaller gains for shorter event sequences. This behavior is expected, as the prefix scan yields more speedup as the sequence length grows. Moreover, our approach successfully fits models on substantially larger subsets, up to approximately 3.2×10^7 events. To the best of our knowledge, this is the first time

Subset	Nodes	Events	Log Lik.	Avg. Epoch Time	
				Ours	Lazy MHP
Bail Out	835	64,138	3.612	0.06 s	0.47 s
Miami Heat	1,173	133,451	1.680	0.21 s	1.60 s
Amy Winehouse	1,561	226,247	2.043	0.34 s	3.30 s
Arab Spring	1,377	400,199	2.796	0.46 s	4.60 s
Greece	1,925	1,077,125	2.280	1.24 s	—
Libya	2,003	2,486,030	2.679	2.97 s	—
Crisis	2,266	5,085,759	2.495	6.94 s	—
Leader	2,344	10,604,129	2.674	14.91 s	—
North Korea...	2,451	16,408,957	2.747	23.73 s	—
Prince William...	2,494	32,687,780	2.827	48.33 s	—

Table 2: Summary of MemeTracker subsets and fitted Hawkes process models. Per-event log-likelihood is reported. Lazy MHP results are obtained from Nickel and Le (2021) and are omitted for subsets not considered in the paper.

the standard multivariate Hawkes process, fit via exact maximum likelihood estimation, has been applied to data at this scale.

4.5 Chicago Crime Data

Finally, to demonstrate an analysis at a previously infeasible scale, we fit multivariate Hawkes processes to incident-level data of crimes committed in Chicago. Crimes exhibit strong short-term cross excitation behavior (crimes in an area tend to trigger crimes in neighboring areas), as well as long-term self excitation (crimes in an area influence crimes in the same area), making Hawkes processes well-suited to model crime diffusion (Mohler et al., 2011, 2015; Zhuang and Mateu, 2019).

Every day, the Chicago Police Department (CPD) updates a dataset of all crimes committed from 2001 to the present (Chicago Police Department, 2025). Each crime entry in the dataset has a fine-grained location (at the city block level) and time (accuracy in seconds). We analyze a snapshot of the dataset downloaded on November 14, 2025, containing 8,448,627 crime entries. Since crime spreads differently depending on the type, we extract 5 subsets of the dataset, each containing purely theft, battery, assault, burglary, or robbery crimes. The dimensions of our learned Hawkes processes are which of the 22 Chicago districts the crime occurred in. We use $K = 3$ decay kernels and fit each Hawkes process for 1000 epochs.

A summary of the data and the results of the fitted Hawkes models are given in Table 3. Maps of the influence of certain districts and learned interaction matrices for selected crime types are shown Figures 4 and 5. When considering all crimes, there is very clear hub-and-spoke structure, whereby two districts (corresponding to rows in the interaction matrix) influence crime in many others. Conversely, each individual crime has different behavior: battery crime influence is sparse and sporadic, while burglary and robbery crimes have strong self-influence, and burglary exhibits a similar hub-and-spoke structure. These learned

Crime Types	Events (N)	Avg. Epoch Time	Log-Likelihood
All	7,834,628	1.012 s	1.012
Selected	4,761,820	0.605 s	0.428
Theft	2,071,626	0.296 s	-0.189
Battery	1,420,739	0.200 s	-1.565
Assault	563,535	0.082 s	-2.720
Burglary	414,073	0.072 s	-2.454
Robbery	291,847	0.051 s	-3.498

Table 3: Summary of Chicago crime data and the fitted Hawkes models with $M = 22$ nodes.

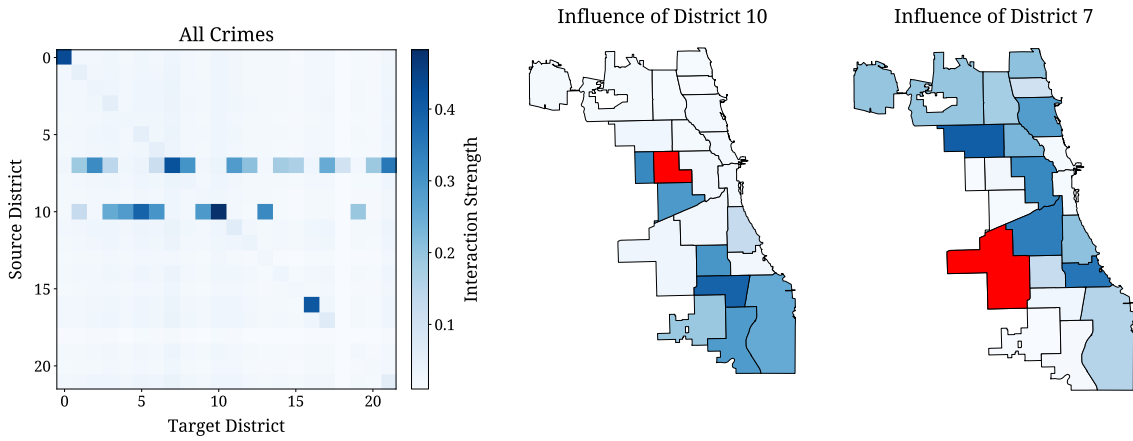


Figure 4: Interaction matrix for all crime types learned from Chicago crime data. Choropleth maps showing influence of particularly influential districts (District 7 and District 10).

patterns are consistent with known spatial crime in Chicago. In particular, districts 7 and 10 (Englewood and Ogden) are widely recognized crime hotspots, while District 6 (Gresham) has historically experienced elevated violent crime rates relative to other districts (Chicago Police Department, 2024).

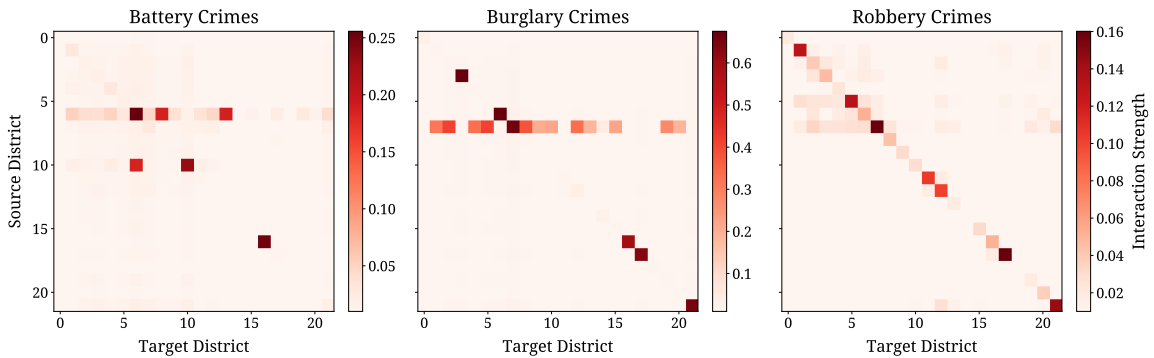


Figure 5: Interaction matrices for selected crime types.

5 Conclusion

This work presented an algorithm for maximum likelihood estimation of linear exponential Hawkes processes at previously infeasible scales. The key idea was to use a parallel prefix scan to compute the likelihood, which enables massive parallelization on GPUs. We demonstrated the performance of our approach on synthetic and real-world datasets, observing orders-of-magnitude improvement in fitting time over other comparable methods. We provide an accompanying library that implements our algorithm in PyTorch.

6 Acknowledgements

We gratefully acknowledge funding from the Media Forensics Hub at Clemson University and the use of the Palmetto supercomputer provided through this support.

Appendix A.

In this section, we present the extension of Algorithm 1 to the batched case. That is, the forward and backward passes for training multivariate Hawkes processes using our approach, split across batches. Note that in order to achieve constant memory usage, each batch's forward pass must immediately be followed by its backward pass, to discard intermediate values. Moreover, computation of the $\nabla\mu_p$ gradient does not have to be batched, as it only depends on the intensities $\lambda_{m_i}(t_i)$, which are stored for the backward pass.

Algorithm 2: Batched training of multivariate Hawkes processes, extending Algorithm 1

define PrefixScan $_{\odot}(\cdot)$ **from** Section 2.2
for each epoch ℓ **do**
 $\mathcal{L}, \nabla\alpha_{p,q,k}, \nabla\gamma_k \leftarrow 0$
for each batch b **do**
 FORWARD PASS
 $\{\mathbf{P}_i^k\}_{i \in \mathcal{I}_b} \leftarrow \text{PrefixScan}_{\odot} \left(\{(e^{-\gamma_k \Delta t_i}, e^{-\gamma_k \Delta t_i} \boldsymbol{\alpha}_{:,m_{i-1}})\}_{i \in \mathcal{I}_b} \right)$
 $\tilde{\mathbf{R}}_i^k \leftarrow \mathbf{P}_i^k \tilde{\mathbf{R}}_{(b-1)N_b}^k, \forall i \in \mathcal{I}_b$
 $\boldsymbol{\lambda}(t_i) \leftarrow \boldsymbol{\mu} + \sum_{k=1}^K \gamma_k \mathbf{R}_i^k, \forall i \in \mathcal{I}_b$
 $\mathcal{L} \leftarrow \mathcal{L} + \sum_{i \in \mathcal{I}_b} \log \lambda_{m_i}(t_i)$
store $\{\lambda_{m_i}(t_i)\}_{i \in \mathcal{I}_b}, \{R_{m_i}(t_i)\}_{i \in \mathcal{I}_b}$ for backward pass
 BACKWARD PASS
 $\{\mathbf{V}_i^k\}_{i \in \mathcal{I}_b} \leftarrow \text{PrefixScan}_{\odot} \left(\{(e^{-\gamma_k \Delta t_i}, e^{-\gamma_k \Delta t_i} \mathbf{e}_{m_{i-1}})\}_{i \in \mathcal{I}_b} \right)$
 $\{\mathbf{W}_i^k\}_{i \in \mathcal{I}_b} \leftarrow \text{PrefixScan}_{\odot} \left(\{(e^{-\gamma_k \Delta t_i}, e^{-\gamma_k \Delta t_i} t_{i-1} \boldsymbol{\alpha}_{:,m_{i-1}})\}_{i \in \mathcal{I}_b} \right)$
 $\tilde{\mathbf{K}}_i^k \leftarrow \mathbf{V}_i^k \tilde{\mathbf{K}}_{(b-1)N_b}^k, \forall i \in \mathcal{I}_b$
 $\tilde{\mathbf{L}}_i^k \leftarrow \mathbf{W}_i^k \tilde{\mathbf{L}}_{(b-1)N_b}^k, \forall i \in \mathcal{I}_b$
 $\nabla\alpha_{p,q,k} \leftarrow \nabla\alpha_{p,q,k} + \left. \frac{\partial \mathcal{L}}{\partial \alpha_{p,q,k}} \right|_{i \in \mathcal{I}_b}$ using Equation (9) and $\{\mathbf{K}_i^k\}_{i \in \mathcal{I}_b}$
 $\nabla\gamma_k \leftarrow \nabla\gamma_k + \left. \frac{\partial \mathcal{L}}{\partial \gamma_k} \right|_{i \in \mathcal{I}_b}$ using Equation (10) and $\{\mathbf{L}_i^k\}_{i \in \mathcal{I}_b}, \{R_{m_i}(t_i)\}_{i \in \mathcal{I}_b}$
 $\nabla\mu_p \leftarrow$ using Equation (8) and $\{\lambda_{m_i}(t_i)\}_{i=1}^N$
 $\mu_p, \alpha_{p,q,k}, \gamma_k \leftarrow \text{OptimizerStep}(\mu_p, \alpha_{p,q,k}, \gamma_k, \nabla\mu_p, \nabla\alpha_{p,q,k}, \nabla\gamma_k, \text{lr})$

References

- Yacine Aït-Sahalia, Julio Cacho-Diaz, and Roger J. A. Laeven. Modeling financial contagion using mutually exciting jump processes. *Journal of Financial Economics*, 117(3):585–606, September 2015. ISSN 0304-405X. doi: 10.1016/j.jfineco.2015.03.002.
- Emmanuel Bacry, Iacopo Mastromatteo, and Jean-François Muzy. Hawkes Processes in Finance. *Market Microstructure and Liquidity*, 01(01):1550005, June 2015. ISSN 2382-6266. doi: 10.1142/S2382626615500057.

- Emmanuel Bacry, Martin Bompaire, Stéphane Gaïffas, and Jean-Francois Muzy. Sparse and low-rank multivariate Hawkes processes. *Journal of Machine Learning Research*, 21(50):1–32, 2020. ISSN 1533-7928.
- Albert-László Barabási. Scale-Free Networks: A Decade and Beyond. *Science*, 325(5939):412–413, July 2009. doi: 10.1126/science.1173299.
- Guy E. Blelloch. Prefix Sums and Their Applications. Technical Report CMU-CS-90-190, School of Computer Science, Carnegie Mellon University, November 1990.
- Béla Bollobás, Christian Borgs, Jennifer Chayes, and Oliver Riordan. Directed scale-free graphs. In *Proceedings of the Fourteenth Annual ACM-SIAM Symposium on Discrete Algorithms*, SODA '03, pages 132–139, USA, January 2003. Society for Industrial and Applied Mathematics. ISBN 978-0-89871-538-5.
- Raiha Browning, Deborah Sulem, Kerrie Mengersen, Vincent Rivoirard, and Judith Rousseau. Simple discrete-time self-exciting models can describe complex dynamic processes: A case study of COVID-19. *PLOS ONE*, 16(4):e0250015, April 2021. ISSN 1932-6203. doi: 10.1371/journal.pone.0250015.
- Wen-Hao Chiang, Xueying Liu, and George Mohler. Hawkes process modeling of COVID-19 with mobility leading indicators and spatial covariates. *International Journal of Forecasting*, 38(2):505–520, April 2022. ISSN 0169-2070. doi: 10.1016/j.ijforecast.2021.07.001.
- Chicago Police Department. 2024 Annual Report. Technical report, Chicago Police Department, 2024.
- Chicago Police Department. Crimes - 2001 to Present, 2025.
- Michael Eichler, Rainer Dahlhaus, and Johannes Dueck. Graphical Modeling for Multivariate Hawkes Processes with Nonparametric Link Functions. *Journal of Time Series Analysis*, 38(2):225–242, 2017. ISSN 1467-9892. doi: 10.1111/jtsa.12213.
- Paul Embrechts, Thomas Liniger, and Lu Lin. Multivariate Hawkes processes: An application to financial data. *Journal of Applied Probability*, 48(A):367–378, August 2011. ISSN 0021-9002, 1475-6072. doi: 10.1239/jap/1318940477.
- Jalal Etesami, Negar Kiyavash, Kun Zhang, and Kushagra Singhal. Learning network of multivariate Hawkes processes: A time series approach. In *Proceedings of the Thirty-Second Conference on Uncertainty in Artificial Intelligence*, UAI'16, pages 162–171, Arlington, Virginia, USA, June 2016. AUAI Press. ISBN 978-0-9966431-1-5.
- Felipe Gerhard, Moritz Deger, and Wilson Truccolo. On the stability and dynamics of stochastic spiking neuron models: Nonlinear Hawkes process and point process GLMs. *PLOS Computational Biology*, 13(2):e1005390, February 2017. ISSN 1553-7358. doi: 10.1371/journal.pcbi.1005390.
- Manuel Gomez Rodriguez, Jure Leskovec, and Bernhard Schölkopf. Structure and dynamics of information pathways in online media. In *Proceedings of the Sixth ACM International*

- Conference on Web Search and Data Mining, WSDM '13*, pages 23–32, New York, NY, USA, February 2013. Association for Computing Machinery. ISBN 978-1-4503-1869-3. doi: 10.1145/2433396.2433402.
- Alan G. Hawkes. Hawkes processes and their applications to finance: A review. *Quantitative Finance*, 18(2):193–198, February 2018. ISSN 1469-7688. doi: 10.1080/14697688.2017.1403131.
- W. Daniel Hillis and Guy L. Steele. Data parallel algorithms. *Commun. ACM*, 29(12):1170–1183, December 1986. ISSN 0001-0782. doi: 10.1145/7902.7903.
- Matthias Kirchner. An estimation procedure for the Hawkes process. *Quantitative Finance*, 17(4):571–595, April 2017. ISSN 1469-7688. doi: 10.1080/14697688.2016.1211312.
- Ryota Kobayashi and Renaud Lambiotte. TiDeH: Time-Dependent Hawkes Process for Predicting Retweet Dynamics. *Proceedings of the International AAAI Conference on Web and Social Media*, 10(1):191–200, 2016. ISSN 2334-0770. doi: 10.1609/icwsm.v10i1.14717.
- Régis C. Lambert, Christine Tuleau-Malot, Thomas Bessaih, Vincent Rivoirard, Yann Bouret, Nathalie Leresche, and Patricia Reynaud-Bouret. Reconstructing the functional connectivity of multiple spike trains using Hawkes models. *Journal of Neuroscience Methods*, 297:9–21, March 2018. ISSN 0165-0270. doi: 10.1016/j.jneumeth.2017.12.026.
- Rémi Lemonnier, Kevin Scaman, and Argyris Kalogeratos. Multivariate Hawkes Processes for Large-Scale Inference. *Proceedings of the AAAI Conference on Artificial Intelligence*, 31(1), February 2017. ISSN 2374-3468. doi: 10.1609/aaai.v31i1.10846.
- Jure Leskovec, Lars Backstrom, and Jon Kleinberg. Meme-tracking and the dynamics of the news cycle. In *Proceedings of the 15th ACM SIGKDD International Conference on Knowledge Discovery and Data Mining, KDD '09*, pages 497–506, New York, NY, USA, June 2009. Association for Computing Machinery. ISBN 978-1-60558-495-9. doi: 10.1145/1557019.1557077.
- Erik Lewis and George Mohler. A Nonparametric EM Algorithm for Multiscale Hawkes Processes. *Journal of Nonparametric Statistics*, January 2011.
- G. O. Mohler, M. B. Short, P. J. Brantingham, F. P. Schoenberg, and G. E. Tita. Self-Exciting Point Process Modeling of Crime. *Journal of the American Statistical Association*, 106(493):100–108, March 2011. ISSN 0162-1459. doi: 10.1198/jasa.2011.ap09546.
- G. O. Mohler, M. B. Short, Sean Malinowski, Mark Johnson, G. E. Tita, Andrea L. Bertozzi, and P. J. Brantingham. Randomized Controlled Field Trials of Predictive Policing. *Journal of the American Statistical Association*, 110(512):1399–1411, October 2015. ISSN 0162-1459. doi: 10.1080/01621459.2015.1077710.
- Maximilian Nickel and Matthew Le. Modeling Sparse Information Diffusion at Scale via Lazy Multivariate Hawkes Processes. In *Proceedings of the Web Conference 2021, WWW '21*, pages 706–717, New York, NY, USA, June 2021. Association for Computing Machinery. ISBN 978-1-4503-8312-7. doi: 10.1145/3442381.3450094.

- Y. Ogata. On Lewis' simulation method for point processes. *IEEE Transactions on Information Theory*, 27(1):23–31, January 1981. ISSN 1557-9654. doi: 10.1109/TIT.1981.1056305.
- Yosihiko Ogata. Statistical Models for Earthquake Occurrences and Residual Analysis for Point Processes. *Journal of the American Statistical Association*, 83(401):9–27, March 1988. ISSN 0162-1459. doi: 10.1080/01621459.1988.10478560.
- Yosihiko Ogata. Space-Time Point-Process Models for Earthquake Occurrences. *Annals of the Institute of Statistical Mathematics*, 50(2):379–402, June 1998. ISSN 1572-9052. doi: 10.1023/A:1003403601725.
- Marian-Andrei RizoIU, Young Lee, Swapnil Mishra, and Lexing Xie. Hawkes processes for events in social media. In *Frontiers of Multimedia Research*, volume 17, pages 191–218. Association for Computing Machinery and Morgan & Claypool, December 2017a. ISBN 978-1-970001-07-5.
- Marian-Andrei RizoIU, Lexing Xie, Scott Sanner, Manuel Cebrian, Honglin Yu, and Pascal Van Hentenryck. Expecting to be HIP: Hawkes Intensity Processes for Social Media Popularity. In *Proceedings of the 26th International Conference on World Wide Web, WWW '17*, pages 735–744, Republic and Canton of Geneva, CHE, April 2017b. International World Wide Web Conferences Steering Committee. ISBN 978-1-4503-4913-0. doi: 10.1145/3038912.3052650.
- Wilson Truccolo. From point process observations to collective neural dynamics: Non-linear Hawkes process GLMs, low-dimensional dynamics and coarse graining. *Journal of Physiology-Paris*, 110(4, Part A):336–347, November 2016. ISSN 0928-4257. doi: 10.1016/j.jphysparis.2017.02.004.
- H. Juliette T. Unwin, Isobel Routledge, Seth Flaxman, Marian-Andrei RizoIU, Shengjie Lai, Justin Cohen, Daniel J. Weiss, Swapnil Mishra, and Samir Bhatt. Using Hawkes Processes to model imported and local malaria cases in near-elimination settings. *PLOS Computational Biology*, 17(4):e1008830, April 2021. ISSN 1553-7358. doi: 10.1371/journal.pcbi.1008830.
- Alejandro Veen and Frederic P Schoenberg. Estimation of Space–Time Branching Process Models in Seismology Using an EM–Type Algorithm. *Journal of the American Statistical Association*, 103(482):614–624, June 2008. ISSN 0162-1459. doi: 10.1198/016214508000000148.
- Ke Zhou, Hongyuan Zha, and Le Song. Learning Social Infectivity in Sparse Low-rank Networks Using Multi-dimensional Hawkes Processes. In *Proceedings of the Sixteenth International Conference on Artificial Intelligence and Statistics*, pages 641–649. PMLR, April 2013.
- Jiancang Zhuang and Jorge Mateu. A Semiparametric Spatiotemporal Hawkes-Type Point Process Model with Periodic Background for Crime Data. *Journal of the Royal Statistical Society Series A: Statistics in Society*, 182(3):919–942, June 2019. ISSN 0964-1998. doi: 10.1111/rssa.12429.

Jiancang Zhuang, Yosihiko Ogata, and David Vere-Jones. Stochastic Declustering of Space-Time Earthquake Occurrences. *Journal of the American Statistical Association*, 97(458): 369–380, June 2002. ISSN 0162-1459. doi: 10.1198/016214502760046925.